Electronic Supplementary Information

Slow magnetic relaxation in hexacoordinated cobalt(II) field-induced single-ions magnets with large spin-reversal barrier

Anna Świtlicka[a], Barbara Machura[a], Mateusz Penkala[b], Alina Bieńko*[c], Dariusz C. Bieńko[d],*

Ján Titiš[e], Cyril Rajnák[e], Roman Boča[e], Andrew Ozarowski[f]

[a] Department of Crystallography, Institute of Chemistry, University of Silesia, 9 Szkolna St., 40-006 Katowice, Poland, E-mail: anna.switlicka@us.edu.pl

[b] Department of Inorganic, Organometallic Chemistry and Catalysis, Institute of Chemistry, University of Silesia, 9th Szkolna St., 40-006 Katowice, Poland.

[c] Faculty of Chemistry, University of Wroclaw, 14 F. Joliot-Curie, 50-383 Wroclaw, Poland E-mail: alina.bienko@chem.uni.wroc.pl

[d] Faculty of Chemistry, Wroclaw University of Technology, Wybrzeze Wyspiańskiego 27, 50-370 Wroclaw, Poland

[e] Department of Chemistry, Faculty of Natural Sciences, University of SS Cyril and Methodius, 917 01 Trnava, Slovakia

Abbreviations
1, $[Co(pypz)(H_2O)(dca)]\cdot(dca)$
2, $[Co_2(pypz)_2(\mu_{1,1}\text{-}N_3)_2(N_3)_2]\cdot CH_3OH$
3, $[Co(pypz)_2](tcm)_2$

Experimental section

Materials and General Methods. 2,6-bis(pyrazol–1–yl)pyridine (*pypz*) was synthesised according to the literature method. [1] The other reagents were commercially available and they were used without further purification. IR spectra were recorded on a Nicolet iS5 FT–IR spectrophotometer in the spectral range 4000–400cm^{-1} with the samples in the form of KBr pellets. The electronic spectra were obtained from solid state samples on Nicolet Evolution 220 (190–1100 nm) and Nicolet iS50 FT–IR (700 – 1500 nm) spectrophotometers. X–ray powder diffraction (XRPD) measurements were performed on a PANalytical Empyrean X–ray diffractometer by using Cu−K_α radiation (λ = 1.5418 Å), in which the X–ray tube was operated at 40 kV and 30 mA ranging from 5 to 50°. Elemental analyses (C/H/N) were performed on a Vario EL III analyzer.

Synthesis of $[Co(pypz)(H_2O)(dca)]\cdot(dca)$ (1). $NaN(CN)_2$ (0.075 g, 0.84 mmol) dissolved in water (10 cm^3) was slowly added to a deep pink methanol solution of $CoCl_2\cdot 6H_2O$ (0.10 g, 0.42 mmol). Solid organic ligand *pypz* (0.09 g, 0.42 mmol) was poured into the resulting solution during continuous stirring for 15 min. The mother liquor was left to slow evaporation at room temperature and X–ray quality purple prisms of **1** were formed after a few days. They were collected by filtration and dried in the open air. Yield *ca.* 65%. IR (KBr/cm^{-1}): 3262(m) [ν(OH)], 2316(vs) [ν_{as} + $\nu_s(C\equiv N)_{dca}$], 2258 (s) [$\nu_{as}(C\equiv N)$], 2146(s) [$\nu_s(C\equiv N)_{dca}$], 1477(m), 1404(m), 1366(m) [$\nu(C=N)_{pypz}$ and $\nu(C=C)_{pypz}$]. Anal. Calc. for $C_{15}H_{11}N_{11}OCo$ (**1**): C, 42.87; H, 2.64; N, 36.66%. Found: C, 42.54; H, 2.68, N 36.66%.

Synthesis of $[Co_2(pypz)_2(\mu_{1,1}\text{-}N_3)_2(N_3)_2]\cdot CH_3OH$ (2). NaN_3 (0.055 g, 0.84 mmol) and $CoCl_2\cdot 6H_2O$ (0.10 g, 0.42 mmol) dissolved in water (25 cm^3) was slowly added to a methanolic solution of ligand *pypz* (0.09 g, 0.42 mmol). The resulting solution was continuously stirring for 15 min, and then the mother liquor was left to slow evaporation at room temperature. X–ray quality pink prisms of **2** were formed after a few days. They were collected by filtration and dried in the open air. Yield *ca.* 60%. IR (KBr/cm^{-1}): 2094(m), 2060(s) [$\nu(C=N_{N3})$], 1473(s), 1402(m), 1342(m) [$\nu(C=N)_{pypz}$ and $\nu(C=C)_{pypz}$]. Anal. Calc. for $C_{24}H_{26}N_{22}O_2Co_2$ (**2**): C, 37.32; H, 3.39; N, 39.89%. Found: C, 37.23; H, 3.45, N 39.33%.

Synthesis of $[Co(pypz)_2](tcm)_2$ (3). $KC(CN)_3$ (0.11 g, 0.84 mmol) dissolved in water (10 cm^3) was slowly added to a methanol solution of $CoCl_2\cdot 6H_2O$ (0.10 g, 0.42 mmol) and ligand *pypz* (0.18 g, 0.84 mmol). The resulting solution during continuous stirring for 15 min. The mother liquor was left to slow evaporation at room temperature and X–ray suitable pink prisms of **3** were formed after a few days. They were collected by filtration and dried in the open air. Yield *ca.* 65 %. IR (KBr/cm^{-1}): 2165(vs) [$\nu(C=N_{tcm})$], 1485(m), 1407(m), 1348(m) [$\nu(C=N)_{pypz}$ and $\nu(C=C)_{pypz}$]. Anal. Calc. for $C_{30}H_{18}N_{16}Co$ (**1**): C, 54.47; H, 2.74; N, 33.88%. Found: C, 53.48; H, 2.89, N 33.51%.

Magnetic measurements. Variable temperature (2 – 300 K) direct current (DC) magnetic susceptibility measurements under applied field of B = 0.01 (T < 20 K) and 0.1 T ($T \geq$ 20 K) and variable– field (0 – 7 T) magnetization measurements at low temperatures in the range 2–7 K were carried out with SQUID magnetometer (Quantum Design). Variable–temperature (2–8 K) alternating current (AC) magnetic susceptibility measurements under different applied static fields in the range of B_{DC} = 0 – 1.0 T were carried out with PPMS system (Quantum Design). The magnetic susceptibility data was corrected for the diamagnetism of the constituent atoms and the sample holder. DC and AC measurements were carried out by crushing the crystals and restraining the sample in order to prevent any displacement due to its magnetic anisotropy.

Crystal structure determination and refinement. Single crystal X–ray diffraction data of **1–3** were collected on a Gemini A Ultra diffractometer equipped with Atlas CCD detector and graphite monochromated Mo$K\alpha$ radiation (λ = 0.71073Å) at room temperature. The unit cell determination and data integration were carried out using the CrysAlis package of Oxford Diffraction. [2] Lorentz, polarization and empirical absorption correction using spherical harmonics implemented in SCALE3 ABSPACK scaling algorithm were applied. [3] The structures were solved by the direct methods using SHELXS97 and refined by full–matrix least–squares on F^2 using SHELXL97 [4]. All non–hydrogen atoms were refined anisotropically. The hydrogen atoms were placed in calculated positions refined using idealized geometries (riding model) and assigned fixed isotropic displacement parameters, d(C–H) = 0.93 Å, U_{iso}(H) = 1.2 U_{eq}(C) (for aromatic); and d(C–H) = 0.96 Å, U_{iso}(H) = 1.5 U_{eq}(C) (for methyl). The methyl groups were allowed to rotate about their local threefold axis.

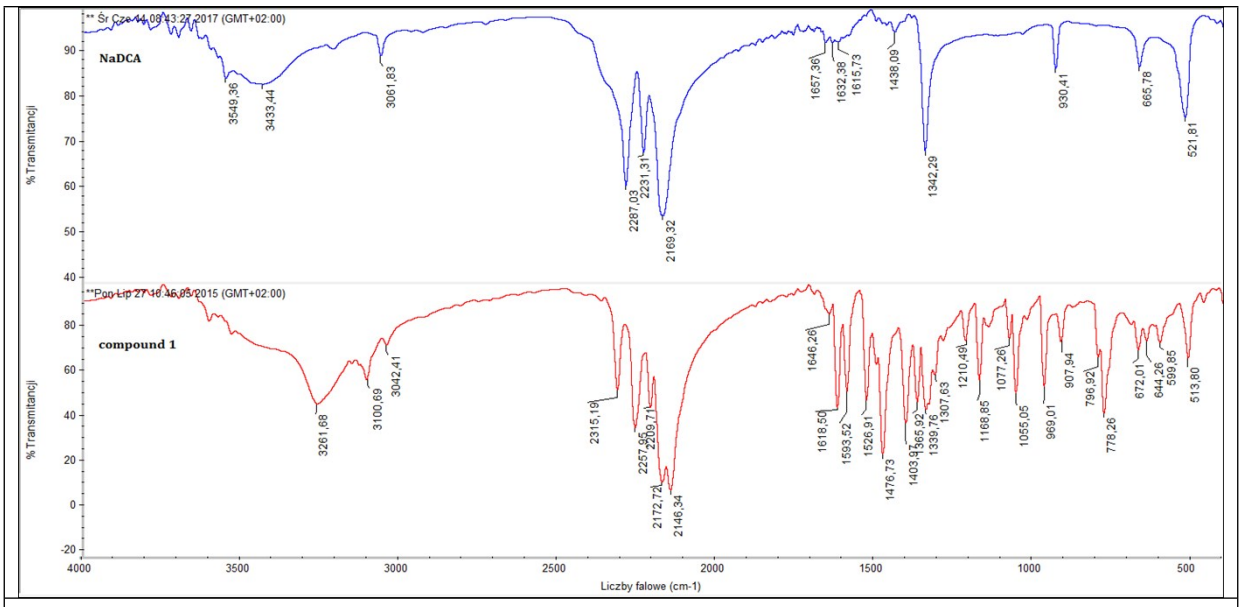

1

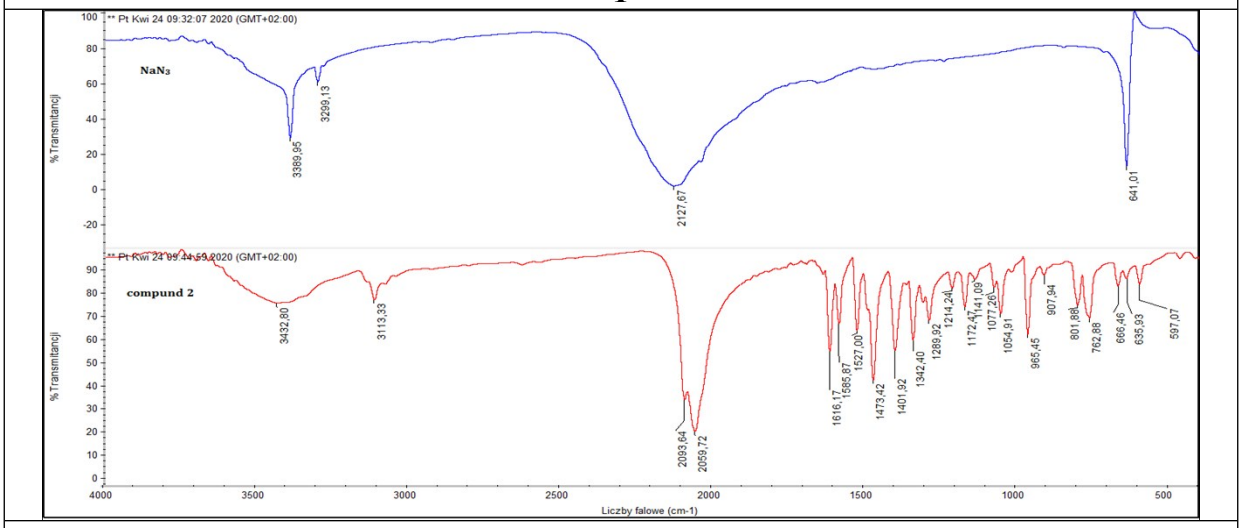

2

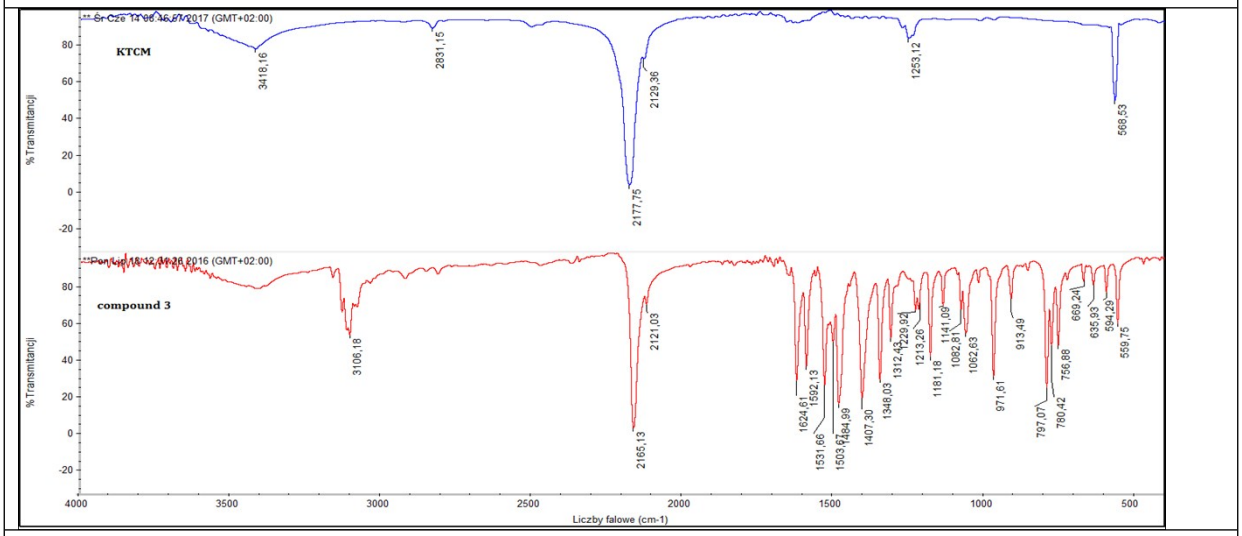

3

Figure S1. IR spectra for **1-3**.

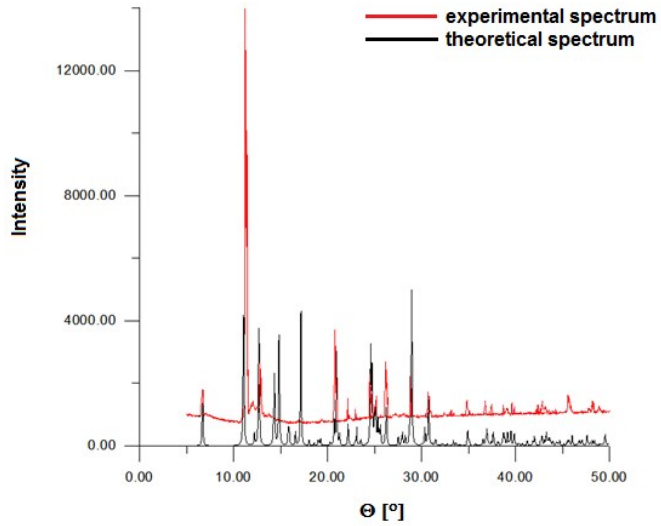

Figure S2. X–ray powder diffraction pattern of **1** at room temperature, together with the calculated pattern from the single crystal data.

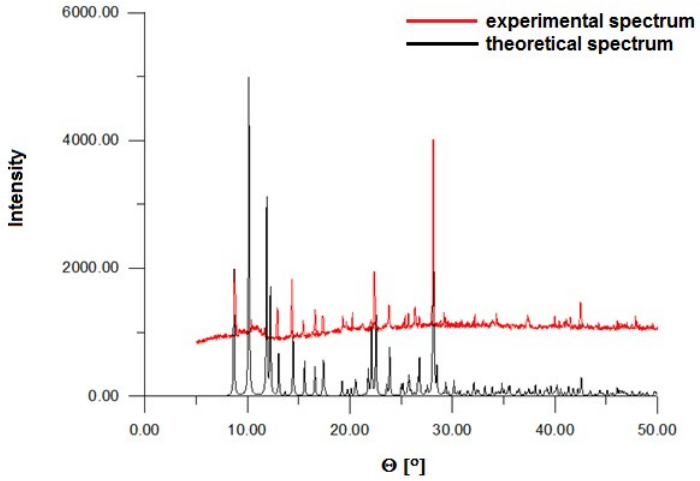

Figure S3. X–ray powder diffraction pattern of **2** at room temperature, together with the calculated pattern from the single crystal data.

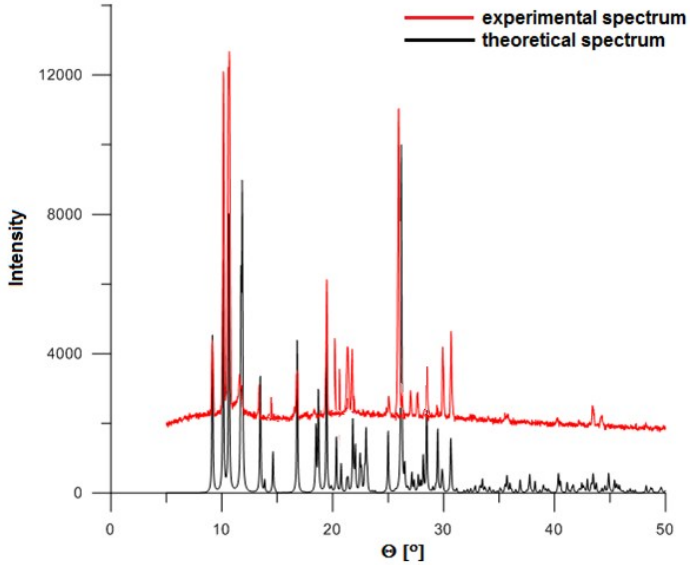

Figure S4. X–ray powder diffraction pattern of **3** at room temperature, together with the calculated pattern from the single crystal data.

Table S1 Crystal data and structure refinement for **1–3**

	1	**2**	**3**
Empirical formula	$C_{15}H_{11}N_{11}OCo$	$C_{24}H_{26}N_{22}O_2Co_2$	$C_{30}H_{18}N_{16}Co$
Formula weight	420.28	772.53	661.53
Temperature [K]	293.0(2)	293.0(2)	293.0(2)
Wavelength [Ĺ]	0.71073	0.71073	0.71073
Crystal system	triclinic	monoclinic	monoclinic
Space group	$P\bar{1}$	$P2_1/c$	$C2/c$
Unit cell dimensions [Ĺ, °]	a = 7.4447(4)	a = 10.2015(6)	a = 19.3070(6)
	b = 8.4287(5)	b = 10.9311(6)	b = 9.2046(4)
	c = 14.6915(7)	c = 14.4944(8)	c = 17.4641(7)
	α = 105.661(5)		
	β = 98.157(5)	β = 94.483(6)	β = 91.643(3)
	γ = 98.189(5)		
Volume [Ĺ^3]	862.73(8)	1611.38(16)	3102.3(2)
Z	2	2	4
Density (calculated) [Mg/m^3]	1.618	1.592	1.416
Absorption coefficient [mm^{-1}]	1.029	1.093	0.603
F(000)	426	788	1348
Crystal size [mm]	0.22 x 0.19 x 0.11	0.15 x 0.13 x 0.04	0.30 x 0.17 x 0.09
θ range for data collection [°]	3.41 to 25.05	3.38 to 25.05	3.36 to 25.05
Index ranges	$-8 \le h \le 7$	$-10 \le h \le 12$	$-22 \le h \le 22$
	$-9 \le k \le 10$	$-13 \le k \le 11$	$-9 \le k \le 10$
	$-17 \le l \le 17$	$-17 \le l \le 16$	$-15 \le l \le 20$
Reflections collected	7081	8718	7176
Independent reflections	3037 (R_{int}=0.0405)	2846 (R_{int} = 0.0383)	2739 (R_{int} = 0.0240)
Completeness to 2θ [%]	99.7	99.8	99.7
Max. and min. transmission	1.00 and 0.831	1.00 and 0.704	1.00 and 0.804
Data / restraints / parameters	3037 / 0 / 254	2846 / 0 / 228	2739 / 0 / 213
Goodness–of–fit on F^2	1.066	1.050	1.051
Final R indices [$I > 2\sigma(I)$]	R_1 = 0.0335	R_1 = 0.0317	R_1 = 0.0328
	wR_2 = 0.0827	wR_2 = 0.0825	wR_2 = 0.0763
R indices (all data)	R_1 = 0.0442	R_1 = 0.0428	R_1 = 0.0424
	wR_2 = 0.0787	wR_2 = 0.0780	wR_2 = 0.0810
Largest diff. peak and hole [e Ĺ$^{-3}$]	0.273 and –0.395	0.324 and –0.254	0.216 and -0.224
CCDC code	1973544	1973545	1973546

Table S2. Selected bond lengths [Å] and angles [°] for **1–3**

Bond lengths		Bond angles	
		1	
Co(1)–N(1)	2.1082(18)	N(1)–Co(1)–N(2)	73.83(7)
Co(1)–N(2)	2.1891(19)	N(1)–Co(1)–N(4)	74.17(7)
Co(1)–N(4)	2.1685(18)	N(1) –Co(1)–O(1)	85.39(7)
Co(1)–N(97)	2.057(2)	N(1)–Co(1)–N(97)	166.05(7)
Co(1)–N(99)	2.096(2)	N(1)–Co(1)–N(99)	95.76(7)
Co(1)–O(1)	2.1338(16)	N(2)–Co(1)–O(1)	91.06(7)
		N(2)–Co(1)–N(4)	147.99(7)
		N(3)–Co(1)–N(97)	97.88(7)
		N(2)–Co(1)–N(99)	90.90(8)
		N(4)–Co(1)–N(97)	113.59(8)
		N(4)–Co(1)–N(99)	91.74(7)
		N(4)–Co(1)–O(1)	86.93(6)
		C(98)–N(97)–Co(1)	155.6(2)
		C(99)–N(99)–Co(1)	165.03(19)
		2	
Co(1)–N(1)	2.0899(17)	N(1)–Co(1)–N(2)	75.00(7)
Co(1)–N(2)	2.1684(19)	N(1)–Co(1)–N(4)	74.47(6)
Co(1)–N(4)	2.1943(18)	N(1)–Co(1)–N(96)	97.29(8)
Co(1)–N(96)	2.065(2)	N(1)–Co(1)–N(99)a	87.40(7)
Co(1)–N(99)	2.0709(17)	N(1)–Co(1)–N(99)	165.11(7)
Co(1)–N(99)a	2.2320(19)	N(2)–Co(1)–N(4)	149.48(7)
		N(2)–Co(1)–N(96)	92.65(9)
		N(2)–Co(1)–N(99)a	91.74(7)
		N(2)–Co(1)–N(99)	101.54(7)
		N(96)–Co(1)–N(4)	91.40(9)
		N(96)–Co(1)–N(99)	97.34(8)
		N(96)–Co(1)–N(99)a	174.27(8)
		N(99)–Co(1)–N(4)a	86.68(7)
		N(99)–Co(1)–N(4)	107.92(7)
		N(99)–Co(1)–N(99)a	78.16(7)
		3	
Co(1)–N(1)	2.0825(14)	N(1)–Co(1)–N(1c)	171.72(8)
Co(1)–N(1)c	2.0825(14)	N(1)–Co(1)–N(2c)	111.51(6)
Co(1)–N(2)	2.1622(17)	N(1)–Co(1)–N(4c)	74.47(6)
Co(1)–N(2)c	2.1622(17)	N(1)–Co(1)–N(4)	99.77(6)
Co(1)–N(4)	2.1605(17)	N(1c)–Co(1)–N(4c)	99.77(6)
Co(1)–N(4)c	2.1605(17)	N(1c)–Co(1)–N(4)	74.47(6)
		N(2)–Co(1)–N(2c)	94.66(9)
		N(4c)–Co(1)–N(4)	94.55(9)
		N(1)–Co(1)–N(2)	74.41(6)
		N(1c)–Co(1)–N(2c)	74.41(6)
		N(1c)–Co(1)–N(2)	111.51(6)
		N(4c)–Co(1)–N(2)	148.72(6)
		N(4)–Co(1)–N(2c)	148.72(6)
		N(4)–Co(1)–N(2)	93.73(7)
		N(4c)–Co(1)–N(2c)	93.73(7)

Symmetry transformations used to generate equivalent atoms: (a): -*x*, -*y*, 2-*z*; (b): 1-*x*, *y*, 1/2-*z*; (c): 1-*x*, *y*, 3/2-*z*

Table S3. Dicyanoamide cobalt(II) complexes with tridendate N–donor ligands

Compound		Co-N_{pypz} [Å]	Co–O_{water} [Å]	Co-N_{dca} [Å]	Co···Co [Å]	Magnetic parameters	Ref
single μ–$_{1,5}$–dca							
$[Co(dca)_2(L^1)]_n$	1D	2.086(2) 2.240(2) 2.154(2)	–	2.164(2) 2.098(2)	8.542	J = –0.35 cm^{-1}	5
$[Co(dca)(L^2)(H_2O)](dca)$	1D	2.213(2) 2.078(2) 2.221(2)	2.005(2)	2.096(2) 2.104(2)	8.465	θ = 7.97 K	6
$[Co(dca)_2(L^3)]_n$	1D	2.157(1) 2.095(2) 2.134(2)	–	2.165(4) 2.035(1)	8.020	–	7
double μ–$_{1,5}$–dca							
$[Co(dca)(L^4)(H_2O)]_2{\cdot}2ClO_4$	dimer	2.087(3) 2.196(3)	2.168(3)	2.108(4) 2.030(4)	7.377(1)	$A\kappa$ = 1.36 $A\kappa\lambda$ = –163 cm^{-1} Δ = 430 cm^{-1}	8
mixed bridges							
$[Co_2(dca)_4(L^2)]_n{\cdot}nCH_3CN$	1D	2.129(2) 2.094(2) 2.142(2)	–	2.026(2) 2.136(2)	8.778	θ = –9.78 K	6
$[Co_2(L^2)(dca)_4]_n$	1D	2.140(2) 2.114(2) 2.156(2)	–	2.044(2) 2.141(2)	7.377	J = –1.10 cm^{-1}	9

L^1 = N,N-diethyl, N'-(pyridin-2-yl)benzylidene)ethane-1,2-diamine; **L^2** = tetra(2-pyridyl)pyrazine; **L^3** = 2,2':6'2"-terpyridine; **L^4** =2,4,6-tri(2-pyridyl)-1,3,5-triazine

Table S4. Azido cobalt(II) complexes with N–donor ligands

Compound	Co-N_L [Å]	Co-N_{N3} [Å]	S(SPY) [a]	S(TBPY) [a]	τ	Magnetic parameters	Ref.
$[Co(L^5)(N_3)_2]$	2.0916(10) 2.1249(10) 2.1191(10)	2.0115(11) 2.0236(11)	2.187	1.076	0.60	–	10
$[Co(L^6)(N_3)]$	2.023(3) 2.187(2) 2.187(2)	1.962(1) 1.962(1)	4.551	2.778	0.41	–	11
$[Co_2(L^7)_2(N_3)_4]$	2.1824(15) 2.0453(16)	1.9751(19) 2.1125(16) 2.0541(18)	4.103	2.026	0.56	J = 10.11 cm^{-1} D = 21.88 cm^{-1}	12
$[Co_2(L^8)_2(N_3)_4]$	2.1534(15) 2.0415(15)	2.1977(15) 2.1977(15) 1.9686(17)	4.333	0.771	0.78	J = 18.1 cm^{-1} zj = –0.84 cm^{-1}	13

L^5= bis(2-(3,5-dimethyl-1H-pyrazol-1-yl)ethyl)amine; **L^6** = 2,4-bis(3,5-dimethyl-1H-pyrazol-1-yl)-6-diethylamino-1,3,5-triazine; **L^7** = 2-(3,5-dimethyl- 1H-pyrazol-1-yl)-4,6-dimethylpyrimidine; **L^8** = 2-(3,5-dimethylpyrazol-1-ylmethyl)pyridine

[a] S(SPY) – square pyramidal shape measure; S(TBPY) – trigonal bipyramid shape measure

AC susceptibility

Fitting of the AC susceptibility data is based upon 44 data points (22 in-phase and 22 out-of-phase) using the formula for the **two-set Debye model**

$$\chi(\omega) = \chi_S + \frac{\chi_{T1} - \chi_S}{1 + (\mathrm{i}\omega\tau_1)^{1-\alpha_1}} + \frac{\chi_{T2} - \chi_{T1}}{1 + (\mathrm{i}\omega\tau_2)^{1-\alpha_2}} \quad \text{or}$$

$$\chi(\omega) = \chi_S + (\chi_T - \chi_S)\left[\frac{x_1}{1 + (\mathrm{i}\omega\tau_1)^{1-\alpha_1}} + \frac{1 - x_1}{1 + (\mathrm{i}\omega\tau_2)^{1-\alpha_2}}\right]$$

where x_1 is the weight of the first, low-frequency relaxation set (channel, branch). This equation decomposes into two explicit formulae for

a) the in-phase component

$$\chi'(\omega) = \chi_S + (\chi_{T1} - \chi_S)\frac{1 + (\omega\tau_1)^{1-\alpha_1}\sin(\pi\alpha_1/2)}{1 + 2(\omega\tau_1)^{1-\alpha_1}\sin(\pi\alpha_1/2) + (\omega\tau_1)^{2-2\alpha_1}}$$

$$+(\chi_{T2} - \chi_{T1})\frac{1 + (\omega\tau_2)^{1-\alpha_2}\sin(\pi\alpha_2/2)}{1 + 2(\omega\tau_2)^{1-\alpha_2}\sin(\pi\alpha_2/2) + (\omega\tau_2)^{2-2\alpha_2}}$$

b) the out-of-phase component

$$\chi''(\omega) = (\chi_{T1} - \chi_S)\frac{(\omega\tau_1)^{1-\alpha_1}\cos(\pi\alpha_1/2)}{1 + 2(\omega\tau_1)^{1-\alpha_1}\sin(\pi\alpha_1/2) + (\omega\tau_1)^{2-2\alpha_1}}$$

$$+(\chi_{T2} - \chi_{T1})\frac{(\omega\tau_2)^{1-\alpha_2}\cos(\pi\alpha_2/2)}{1 + 2(\omega\tau_2)^{1-\alpha_2}\sin(\pi\alpha_2/2) + (\omega\tau_2)^{2-2\alpha_2}}$$

with the constraint for the isothermal susceptibilities $\chi_{T1} < \chi_{T2}$ in order to get positive contributions from each primitive component. Then $x_1 = (\chi_{T1} - \chi_S)/(\chi_{T2} - \chi_S) = (\chi_S - \chi_{T1})/(\chi_S - \chi_{T2})$.

An extension to the three-set Debye model is straightforward.

Seven free parameters (χ_S, χ_{T1}, χ_{T2}, α_1, α_2, τ_1, and τ_2) can be fitted reliably by using 44 experimental data points. The functional to be minimized accounts to the relative errors of both susceptibility components

- $F = w \cdot E(\chi') + (1 - w) \cdot E(\chi'')$ with the typical weight $w = 0.07$, or
- $F = E(\chi') \cdot E(\chi'')$ with $E(\chi) = (1/N)\left[\sum_i^N \left|(\chi_i^{\mathrm{e}} - \chi_i^{\mathrm{c}})/\chi_i^{\mathrm{e}}\right|\right]$

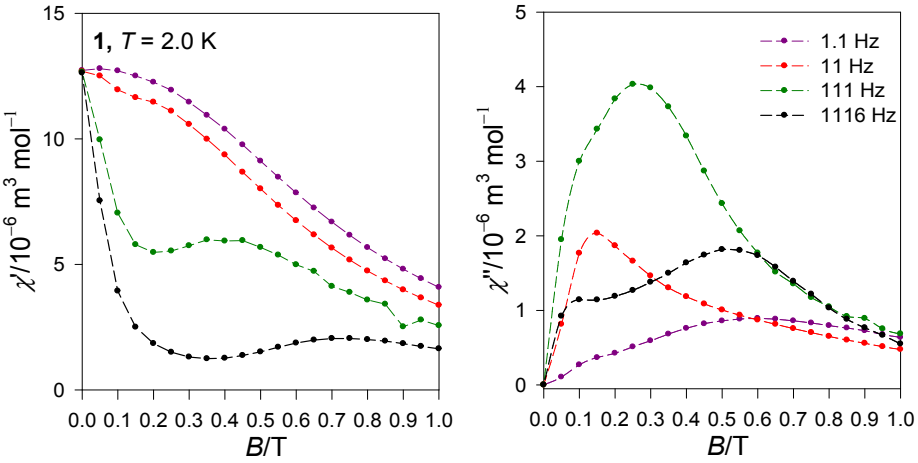

Figure S5. Field dependence of the AC susceptibility components for **1** at T = 2.0 K for a set of frequencies of the AC field. Lines serve as a guide for eyes.

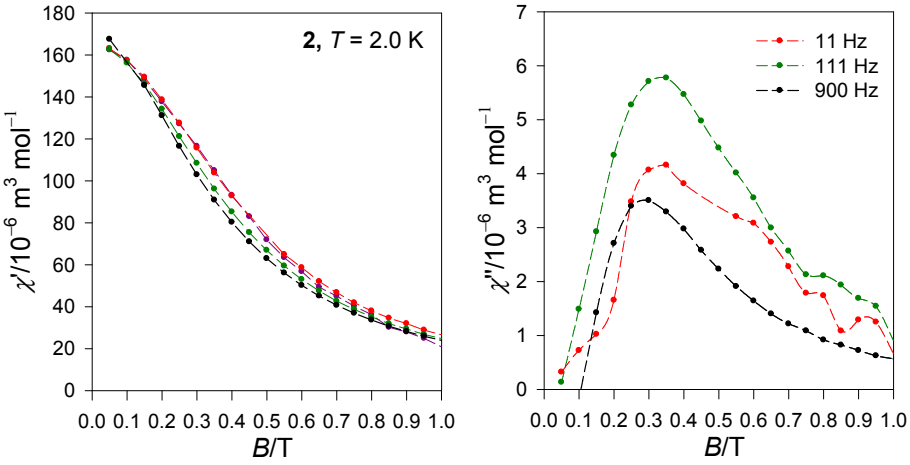

Figure S6. Field dependence of the AC susceptibility components for **2** at T = 2.0 K for a set of frequencies of the AC field. Lines – visual guide.

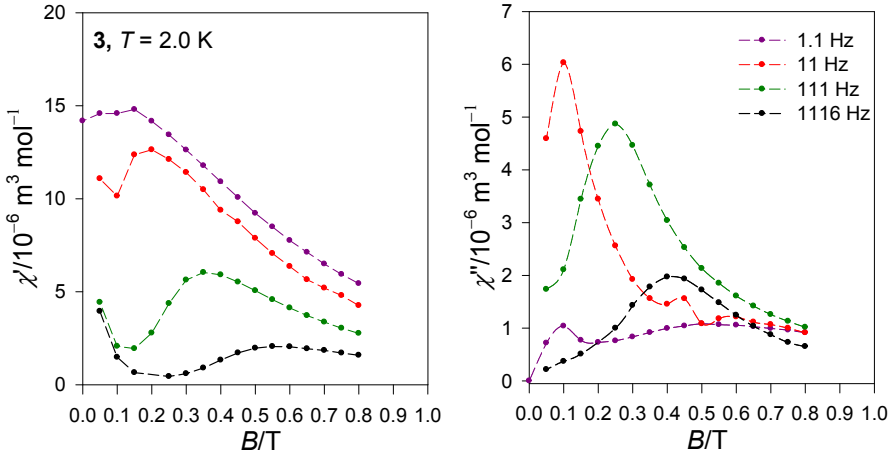

Figure S7. Field dependence of the AC susceptibility components for **3** at T = 2.0 K for a set of frequencies of the AC field. Lines – visual guide.

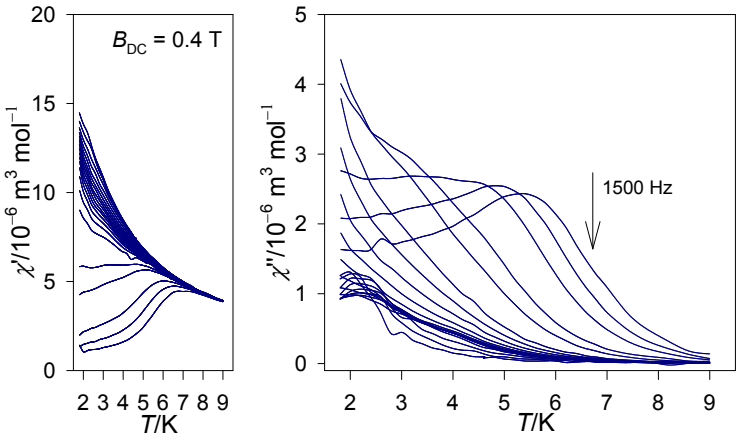

Figure S8. Temperature dependence of the AC susceptibility components for **1** at B_{DC} = 0.4 T and fixed frequency.

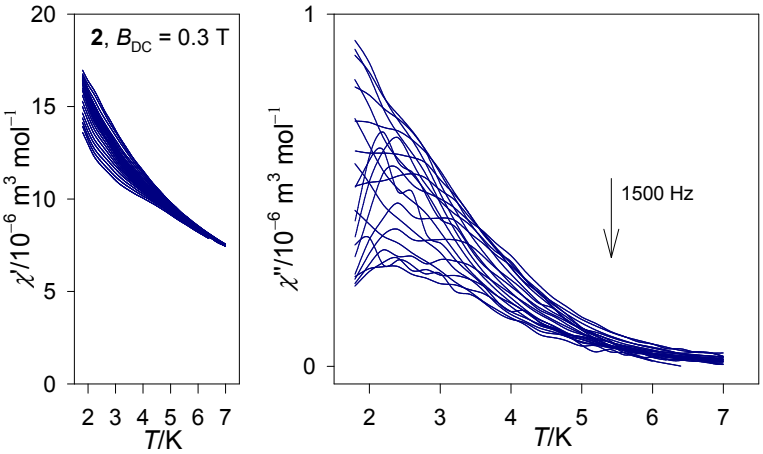

Figure S9. Temperature dependence of the AC susceptibility components for **2** at B_{DC} = 0.3 T and fixed frequency.

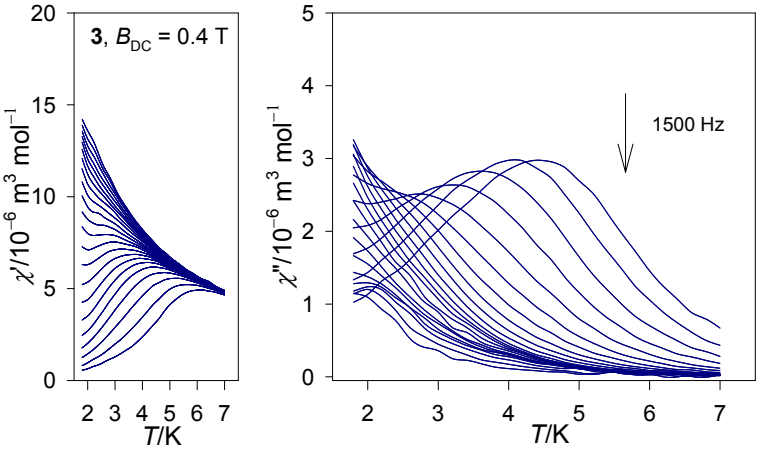

Figure S10. Temperature dependence of the AC susceptibility components for **3** at B_{DC} = 0.3 T and fixed frequency.

Table S5. Results of the fitting procedure for AC susceptibility components of **1** at B_{DC} = 0.4 with a two-set Debye model. [a]

T/K	$R(\chi')$ /%	$R(\chi'')$ /%	χ_{LF}	α_{LF}	τ_{LF} / s	χ_{HF}	α_{HF}	τ_{HF} /10^{-3} s	x_{LF}
1.8	1.1	1.8	5.1(11)	.44(8)	**1.9(10)**	17.1(9)	.21(1)	1.09(2)	.30
2.0	0.91	1.6	5.9(10)	.49(6)	1.8(7)	16.8(8)	.23(1)	0.93(2)	.35
2.2	1.9	1.8	5.4(13)	.48(10)	1.2(7)	15.6(11)	.23(1)	0.84(3)	.35
2.4	1.4	2.5	4.7(7)	.47(7)	0.72(23)	14.3(6)	.23(1)	0.72(2)	.33
2.6	0.49	2.1	3.5(2)	.38(3)	0.40(1)	12.8(11)	.23(1)	0.66(1)	.27
2.8	1.2	2.2	2.5(2)	.27(5)	0.31(3)	11.7(1)	.25(1)	0.62(1)	.21
3.2	0.94	1.9	2.1(2)	.31(5)	0.26(3)	10.6(1)	.24(1)	0.49(1)	.20
3.6	1.9	2.6	1.6(2)	.31(9)	0.19(4)	9.5(1)	.23(1)	0.38(1)	.17
4.0	0.74	2.8	1.4(1)	.34(5)	0.13(2)	8.6(1)	.20(1)	0.29(1)	.16
4.4	0.65	2.7	1.1(1)	.37(5)	0.12(2)	7.9(1)	.17(1)	0.23(1)	.14
5.0	0.89	2.8	0.70(10)	.39(9)	0.10(3)	7.0(1)	.13(1)	0.14(1)	.10
								τ_{HF} /10^{-6} s	
5.8	0.74	1.5	0.41(8)	.47(12)	0.10(4)	6.0(1)	.09(1)	72(1)	.07
6.4	0.28	1.6	0.28(4)	.49(7)	0.11(3)	5.5(1)	.07(1)	41(1)	.05
6.4	0.12	7.0				5.3(1)	.10(1)	41(1)	
7.4	0.72	10				4.7(1)	.11(2)	14(1)	
8.6	0.40	21				4.1(1)	.23(4)	2.0(4)	

[a] χ in units of 10^{-6} m^3 mol^{-1}; χ_S = 0.

Table S6. Results of the fitting procedure for AC susceptibility components of **2** at B_{DC} = 0.3 with a two-set Debye model.

T/K	$R(\chi')$ /%	$R(\chi'')$ /%	χ_S	χ_{LF}	α_{LF}	τ_{LF} / s	χ_{HF}	α_{HF}	τ_{HF} /10^{-3} s	x_{LF}
1.8	0.33	3.9	13.3(1)	14.6(3)	.19(10)	**2.1(8)**	16.8(3)	.33(2)	0.95(4)	.29
2.0	0.19	2.6	12.6(1)	14.2(2)	.22(4)	1.5(2)	17.2(1)	.33(1)	0.82(3)	.36
2.2	0.32	3.0	11.9(1)	13.7(2)	.21(4)	1.1(1)	16.5(1)	.36(2)	0.69(4)	.38
2.6	0.24	2.7	11.0(1)	12.4(1)	.16(4)	0.80(6)	15.2(1)	.42(1)	0.50(3)	.33
3.0	0.28	2.7	10.2(1)	11.2(2)	.13(4)	0.56(4)	13.9(1)	.51(3)	0.31(5)	.28
3.4	0.27	2.0	9.5(2)	10.4(3)	.13(4)	0.45(3)	12.9(3)	.56(4)	0.15(5)	.27
									τ_{HF} /10^{-6} s	
3.8	0.27	3.5	9.0(5)	9.7(6)	.09(5)	0.40(3)	12.0(1)	.63(6)	59(58)	.23
4.2	0.24	3.3	8.5(11)	9.1(11)	.11(7)	0.42(3)	11.2(1)	.69(9)	16(40)	.19
4.6	0.26	4.2	8.2(21)	8.6(21)	.11(9)	0.42(5)	10.5(4)	.70(13)	4.7	.16
5.0	0.22	5.3	7.9(34)	8.1(35)	.05(12)	0.45(5)	9.9(1)	.76(18)	0.90	.12

Table S7. Results of the fitting procedure for AC susceptibility components of **3** at B_{DC} = 0.4 with a three-set (two-set) Debye model.

T/K	$R(\chi')$ /%	$R(\chi'')$ /%	χ_{LF}	α_{LF}	τ_{LF} / s	χ_{IF}	α_{IF}	τ_{IF} /10^{-3} s	χ_{HF}	α_{HF}	τ_{HF} /10^{-3} s	x_{LF}	x_{IF}	x_{HF}
1.8	0.85	2.0	3.6	.46(37)	**0.9(11)**	9.8(29)	.31(21)	13.7(56)	16.0(13)	.27(4)	1.3(5)	.23	.39	.38
2.0	0.62	1.7	3.6	.44(35)	1.5(11)	9.6(30)	.36(22)	14.2(75)	15.5(14)	.28(7)	1.0(4)	.23	.39	.38
2.2	0.83	2.2	3.0	.37(24)	0.74(53)	8.8(44)	.38(26)	10.0(81)	14.1(6)	.26(11)	0.71(32)	.21	.42	.37
2.4	0.75	2.4	4.0(22)	.44(12)	0.20(18)	8.1(22)	.28(22)	4.8(22)	13.0(3)	.22(5)	0.46(13)	.31	.32	.37
2.6	0.65	2.5	3.2(21)	.44(14)	0.21(21)	6.6(14)	.29(22)	5.6(19)	12.3(3)	.22(3)	0.42(7)	.26	.28	.46
2.8	0.70	1.9	1.5(7)	.28(12)	0.32(10)	6.4(19)	.39(13)	4.5(28)	11.3(1)	.15(8)	0.32(3)	.14	.43	.43
3.2	0.69	1.9	0.51(20)	.02(15)	0.38(6)	4.8(8)	.47(6)	4.8(22)	10.0(1)	.09(4)	0.25(1)	.05	.43	.52
3.6	0.53	1.6	0.87	.47(32)	0.29(5)	3.3(7)	.48(11)	4.6(44)	9.2(2)	.09(3)	0.20(1)	.09	.26	.65
4.0	0.24	1.7	1.1(9)	.53(17)	0.17	2.5(5)	.49(8)	1.9	8.5(1)	.05(2)	0.15(1)	.13	.17	.70
4.4	0.25	1.4	0.77	.57(39)	9.26	1.6(6)	.50(39)	3.1	7.8(3)	.05(2)	0.11(1)	.10	.10	.80
					τ_{LF} /10^{-3} s						τ_{HF} /10^{-6} s			
5.0	0.15	1.3	0.78(6)	.59(3)	27(5)				6.8(1)	.04(1)	72(1)	.11	-	.89
5.8	0.19	1.4	0.36(5)	.59(6)	27(8)				5.9(1)	.03(1)	37(1)	.06		.94
6.4	0.30	3.2	0.22(7)	.59(12)	38(23)				5.4(1)	.03(1)	22(1)	.04		.96
7.0	0.21	5.7	0.15(5)	.60(15)	80(62)				4.9(1)	.04(2)	14(1)	.03		.97

χ_S = 0.

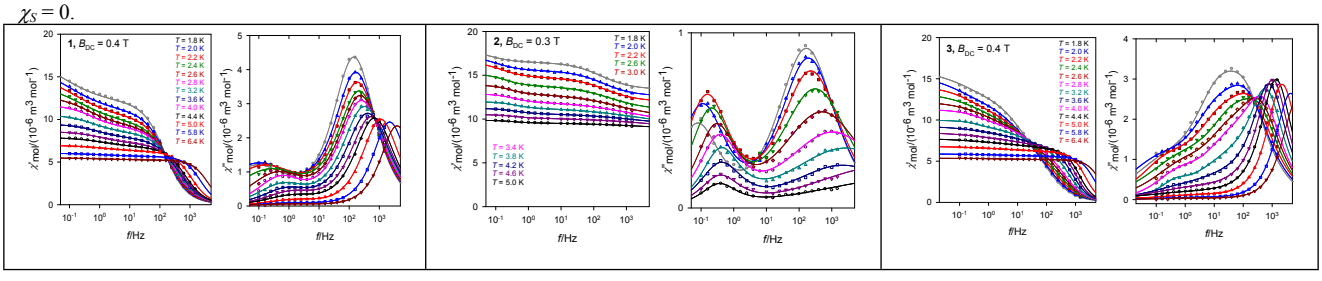

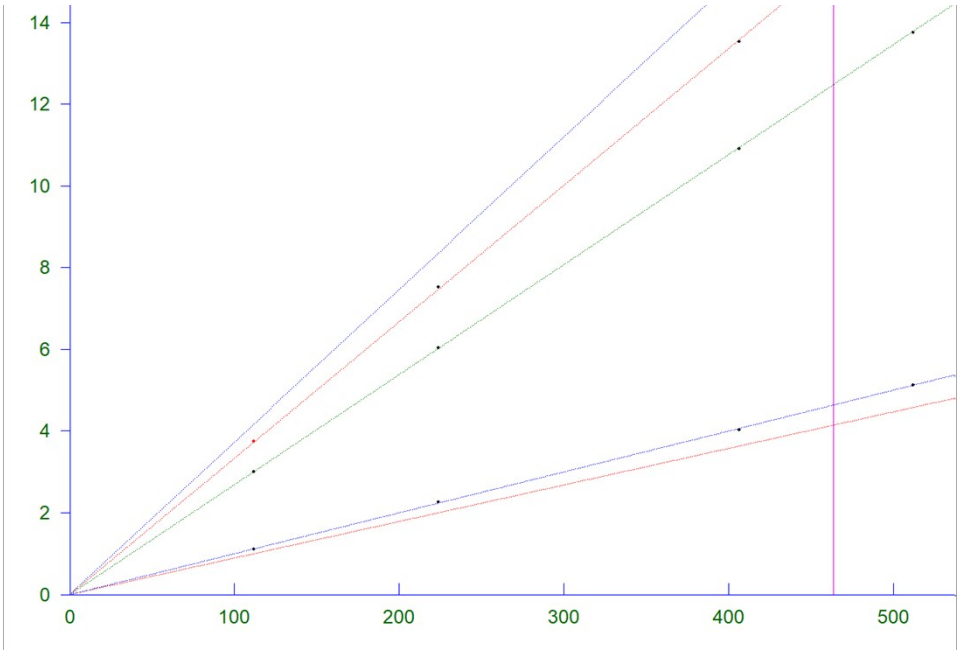

Figure S11. Field (T) *vs* frequency (GHz) map of the resonances observed for **1** at 5 K. The green, blue and red lines correspond to the orientations X, Y and Z, respectively. The lines on which the experimental points are not located represent transitions in the upper Kramers doublet, |±3/2> which with a large positive *D* is not populated.

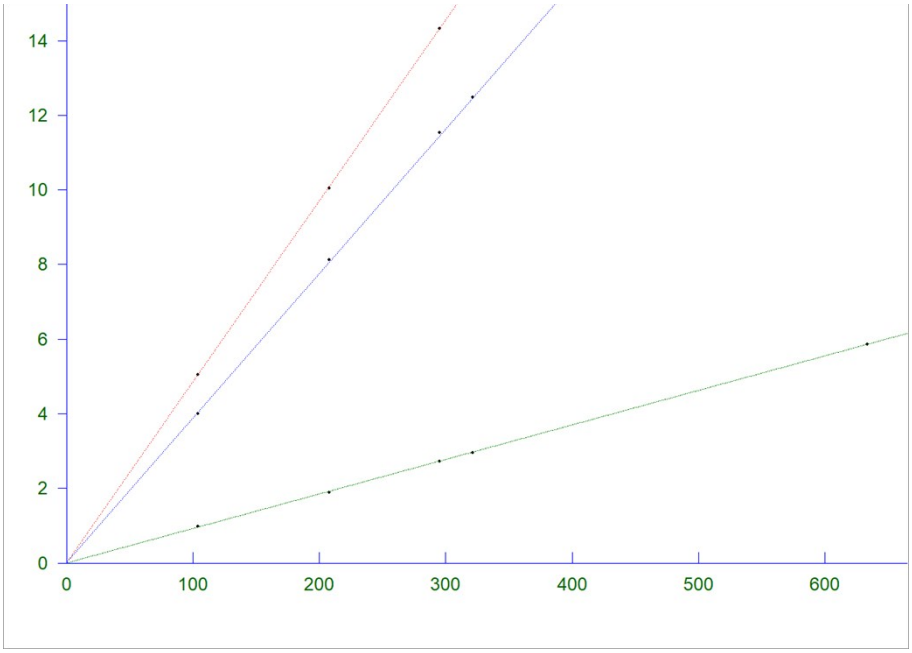

Figure S12. Field (T) *vs* frequency (GHz) map of the resonances observed for **3** at 5 K. The green, blue and red lines correspond to the orientations X, Y and Z, respectively. They can be simulated using an effective $S = 1/2$ state with $g_x = 7.71$, $g_y = 1.84$, $g_z = 1.47$.

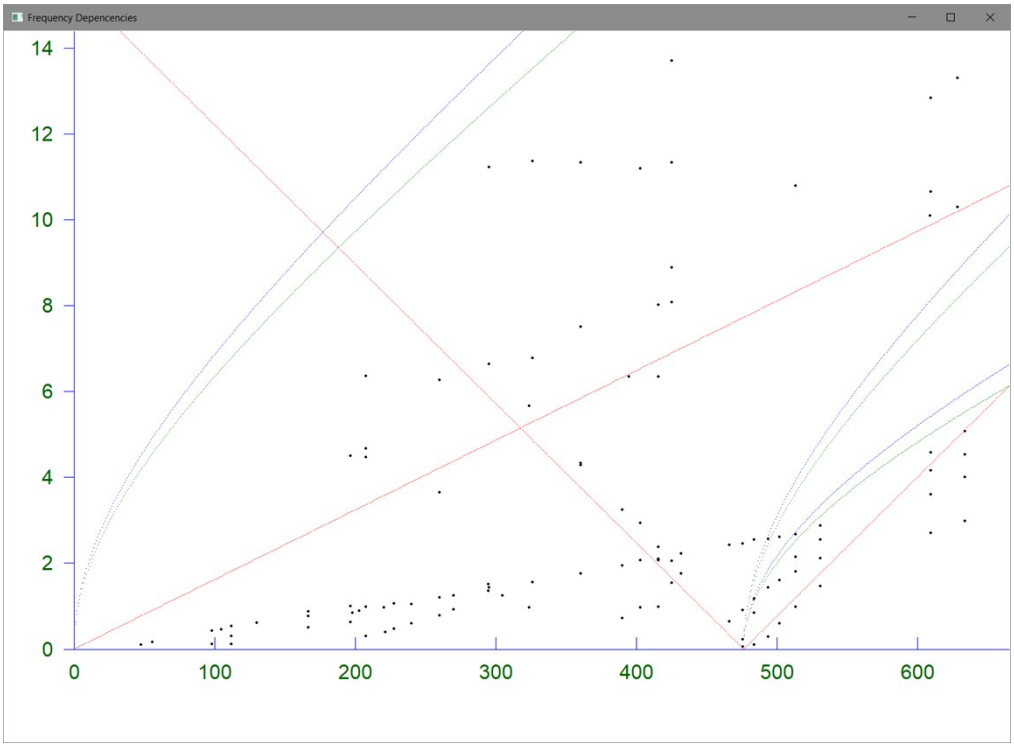

Figure S13. Field (T) *vs* frequency (GHz) map of the resonances observed for **2** at 5 K. The branches marked in red appear to correspond to the ±2> to |±3> transitions at the Z orientation, indicating $g_z = 2.0$ and $D \sim 3.2$ cm^{-1} in the coupled $S = 3$ state.

Table S8. SOC corrected absorption spectrum (energies of the lowest Kramers doublets) by *ab initio* ORCA calculations for **3**

States	Energy (cm-1)	Wavelength (nm)	fosc	T2 (D**2)	|TX| (D)	|TY| (D)	|TZ| (D)
0 1	0.0	0.0	0.000000000	0.00000	0.00000	0.00000	0.00000
0 2	**163.3**	61220.3	0.000000002	0.00007	0.00144	0.00130	0.00801
0 3	**163.3**	61220.3	0.000000001	0.00003	0.00307	0.00292	0.00269
0 4	**702.0**	14244.3	0.000000050	0.00045	0.00975	0.01041	0.01570
0 5	**702.0**	14244.3	0.000000004	0.00004	0.00227	0.00125	0.00562
0 6	**992.7**	10073.3	0.000000284	0.00182	0.02021	0.02121	0.03109
0 7	**992.7**	10073.3	0.000000957	0.00615	0.04098	0.04156	0.05237
0 8	**1474.6**	6781.5	0.000000244	0.00106	0.01505	0.01445	0.02490
0 9	**1474.6**	6781.5	0.000000299	0.00129	0.00243	0.00251	0.03580
0 10	1601.0	6246.2	0.000000102	0.00040	0.00189	0.00143	0.01998
0 11	1601.0	6246.2	0.000000053	0.00021	0.00736	0.00577	0.01108
0 12	8945.9	1117.8	0.000000153	0.00011	0.00618	0.00690	0.00483
0 13	8945.9	1117.8	0.000000128	0.00009	0.00628	0.00676	0.00253
0 14	8975.4	1114.2	0.000000020	0.00001	0.00287	0.00206	0.00131
0 15	8975.4	1114.2	0.000000067	0.00005	0.00378	0.00397	0.00414
0 16	9047.4	1105.3	0.000000151	0.00011	0.00743	0.00699	0.00166
0 17	9047.4	1105.3	0.000000014	0.00001	0.00090	0.00114	0.00273
0 18	9109.9	1097.7	0.000000136	0.00010	0.00523	0.00410	0.00714
0 19	9109.9	1097.7	0.000000280	0.00020	0.00641	0.00619	0.01079
0 20	9868.3	1013.3	0.000000035	0.00002	0.00173	0.00222	0.00383
0 21	9868.3	1013.3	0.000000030	0.00002	0.00200	0.00191	0.00345

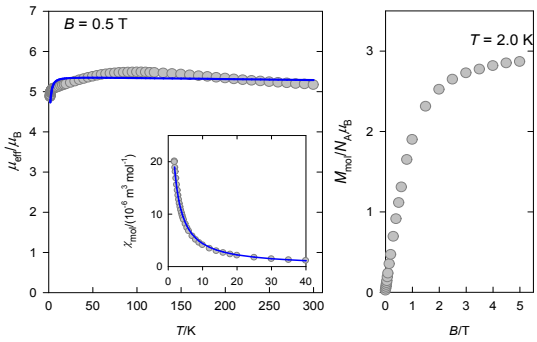

Figure S14. Susceptibility data of **1** fitted in the approximation of a four-membered ring.

REFERENCES

(1) G. Baum, A. J. Blake, D. Fenske, P. Hubberstey, C. Julio and M.A. Withersby, (Acetonitrile)[2,6-bis (pyrazol-1-yl)pyridine](isonicotinamide)copper(II)-tetrafluoroborate-acetonitrile, *Acta Cryst*. **2002**, *C58*, m542–m544.

(2) G. M. Sheldrick, CrysAlis RED, Oxford Diffraction Ltd., Version 1.171.29.2. Phase annealing in SHELX-90: direct methods for larger structures. *Acta Cryst*. **1990**, *A46*, 467–473.

(3) *CrysAlis RED*, Oxford Diffraction Ltd., Version 1.171.35.11. **2011**.

(4) G. M. Sheldrick, A short history of *SHELX*. *Acta Cryst.* **2008**, *A64*, 112–122.

(5) S. Kundu, S. Roy, K. Bhar, R. Ghosh, C.H. Lin, J. Ribas and B. Kumar Ghosh, B. Syntheses, structures and magnetic properties of two one-dimensional coordination polymers of cobalt(II) and nickel(II) dicyanamide containing a tridentate N-donor Schiff base. *J. Mol. Struct*. **2013**, *1038*, 78–85.

(6) J. Luo, L. Qiu, B. Liu, X. Zhang, F. Yang and L. Cui, Synthesis, Structure and Magnetic Properties of Two Cobalt(II) Dicyanamide (dca) Complexes with Heterocyclic Nitrogen Donors Tetra(2-pyridyl)pyrazine (tppz) and 2,4,6-Tri(2-pyridyl)-1,3,5-triazine (tptz): $[Co_2(tppz)(dca)_4]\cdot CH_3CN$ and $[Co(tptz)(dca)(H_2O)](dca)$. *Chin. J. Chem*. **2012**, *30*, 522–528.

(7) H. Yu, *CSD Communication*, **2016**.

(8) A. Das, C. Marschner, J. Cano, J. Baumgartner, J. Ribas, M. Salah El Fallah and S. Mitra, Synthesis, crystal structures and magnetic behaviors of two dicyanamide bridged di- and polynuclear complexes of cobalt(II) derived from 2,4,6-tris(2-pyridyl)1,3,5-triazine and imidazole. *Polyhedron* **2009**, *28*, 2436–2442.

(9) G.Y. Hsu, C.W. Chen, S.C. Cheng, S.H. Lin, H.H. Wei and C.J. Lee, Structure and magnetic properties of one-dimensional metal complexes constructed from alternating dicyanamide linked through binuclear metal tetra-2-pyridylpyrazine subunits. *Polyhedron* **2005**, *24*, 487–494.

(10) S. S. Massoud, F.R. Louka, Y.K. Obaid, R. Vicente, J. Ribas, R.C. Fischerc and F.A. Mautner, Metal ions directing the geometry and nuclearity of azido-metal(II) complexes derived from bis(2-(3,5-dimethyl-1H-pyrazol-1-yl)ethyl)amine. *Dalton Trans*. **2013**, *42*, 3968–3978.

(11) X. Wang, Y. Heng Xing, F. Ying Bai, X. Yu Wang, Q.L. Guan, Y.N. Hou, R. Zhang and Z. Shi, Synthesis, structure, and surface photovoltage properties of a series of novel d^7–d^{10} metal complexes with pincer N-heterocycle ligands. *RSC Adv*. **2013**, *3*, 16021–16033.

(12) A. Jana, S. Konar, K. Das, S. Ray, J. A. Golen, A. L. Rheingold, L. M. Carrella, E. Rentschler, T. K. Mondal, S. K. Kar, Azide bridged dicopper(II), dicobalt(II) complexes and a rare double l-chloride bridged ferromagnetic dicobalt(II) complex of a pyrazolyl-pyrimidine ligand: Synthesis, crystal structures, magnetic and DFT studies, *Polyhedron*, **2012**, *38*, 258–266.

(13) S.Q. Bai, E.Q. Gao, Z. He, C.J. Fang and C. H. Yan, Crystal structures and magnetic behaviour of three new azido-bridged dinuclear cobalt(II) and copper(II) complexes, *New J. Chem*., **2005**, *29*, 935–941.